SiC p+n Junction Diodes Toward Beam Monitor Applications

Tetsuichi Kishishita, Ryoji Kosugi, Yowichi Fujita, Yoshinori Fukao, Kazutoshi Kojima, Keiko Masumoto, Hajime Nishiguchi, Manobu M. Tanaka, and Yasunori Tanaka

***Abstract*— We report on silicon carbide (SiC) p-n junction diodes with a high blocking voltage over 3 kV. Although SiC radiation sensors have been developed with a Schottky barrier type due to a simple fabrication process in the early stages, p-n junction structures are advantageous due to lower sensitivity of the surface defects. Thus, this system provides an ideal condition to investigate the effect of bulk crystal defects on the characteristics of the radiation sensor. The p-n diodes were designed with a device simulator and fabricated with a 4-in 4H-SiC wafer. The epitaxial layer was grown on an n-type substrate with sufficiently low doping concentration of $N_d - N_a = \sim 5 \times 10^{14}$ cm^{-3} and an average thickness of 52 μm. Fabricated p-n diodes with a relatively large leakage current still show a clear peak of the Landau distribution in the charge spectrum, suggesting their practical availability as minimum ionizing particle (MIP) detectors. The estimated electron–hole pair creation energy is consistent with the published studies and we expect good radiation tolerance. Feasibility based on the wafer processing indicates that the prototype devices are a good candidate for the muon beam monitor application in the COherent Muon-to-Electron Transition (COMET) experiment at Japan Proton Accelerator Research Complex (J-PARC).**

***Index Terms*— Beam monitor, minimum ionizing particle (MIP) detectors, p-n diode, semiconductor radiation detectors, silicon carbide (SiC).**

I. Introduction

SILICON carbide (SiC) has been considered as a potential alternative to Si for the manufacture of dosimeters, spectrometers, and charge particle detectors in high-energy physics (HEP) experiments, by virtue of its operation capability in strong radiation and/or high-temperature environments [1], [2]. The potential of SiC as a radiation detector was first discussed by Babcock and coworkers over 60 years ago [3], [4]. Although most of the early works were dominated by issues related to the quality of the crystal, considerable progress in high-purity crystal growth and epitaxial technology was made in the late 1990s. Since then, various SiC devices have been studied intensively to gain a better understanding of the performance of the radiation sensor on the basis of material properties of the SiC itself [5]–[8], along with continuous efforts to improve the process.

Due to the wide bandgap of 3.26 eV and the displacement threshold energy of 22–35 eV, SiC holds a stable charge collection efficiency (CCE) even after a 1-MeV neutron equivalent fluent of 10^{13} n/cm^2. Under the same conditions, current n-type silicon detectors show significant degradation in CCE or leakage current characteristic due to the substrate-type inversion [9]–[11]. On the other hand, SiC has suffered from the relatively low value of the detection thickness and the excessive net doping concentration of the epitaxial layer in commercially available wafers. The thin active layer especially imposes a severe constraint on usage as a minimum ionizing particle (MIP) detector, compared with silicon sensors in HEP experiments. The constraint arises from small-signal charges that are dependent on the electron–hole pair creation energy and proportional to the thickness of the depletion layer. The active area is also limited to <1 cm^2 due to the technological difficulties in defect-free SiC crystal production. This value is much smaller than a typical size of $\approx$100 cm^2 as silicon strip sensors for the HEP experiments. However, the progress of larger SiC substrates and high-quality chemical vapor-deposited thick epitaxial layers has renewed interest in the study of SiC technologies for MIP detectors [12]–[14].

Current diode structures of SiC are concentrated on a basic Schottky type in most of the published works. Surface barrier detectors are easily accessible because the fabrication process is a relatively straightforward technique, and experimental results demonstrated their excellent performance [15], [16]. On the other hand, p-n junctions, or pin structures, had not been much focused as radiation sensors due to the process difficulties, especially unusual high-temperature annealing for dopant activation [11], [17]. Nevertheless, the p-n or pin structures of SiC are expected to provide radiation sensors with low leakage current as the wide bandgap semiconductor in general. This is due to the fact that it has lower surface sensitivity to the active region in wafer processing and/or the avalanche multiplication inside the device to supplements the low signal charges. To take advantage of such properties for

Manuscript received September 7, 2021; revised October 4, 2021; accepted October 4, 2021. Date of publication October 8, 2021; date of current version December 17, 2021. This work was supported by the Tsukuba-Innovation Arena (TIA) under Grant TK20-031 and Grant TK21-055.

Tetsuichi Kishishita is with the Institute of Particle and Nuclear Studies, High Energy Accelerator Research Organization (KEK), Tsukuba 305-0801, Japan, and also with the Department of Accelerator Science, Graduate University for Advanced Studies (SOKENDAI), Hayama 240-0193, Japan (e-mail: kisisita@post.kek.jp).

Ryoji Kosugi, Kazutoshi Kojima, Keiko Masumoto, and Yasunori Tanaka are with the National Institute of Advanced Industrial Science and Technology, Tsukuba 305-8560, Japan.

Yowichi Fujita, Yoshinori Fukao, Hajime Nishiguchi, and Manobu M. Tanaka are with the Institute of Particle and Nuclear Studies, High Energy Accelerator Research Organization (KEK), Tsukuba 305-0801, Japan.

Color versions of one or more figures in this article are available at https://doi.org/10.1109/TNS.2021.3118788.

Digital Object Identifier 10.1109/TNS.2021.3118788

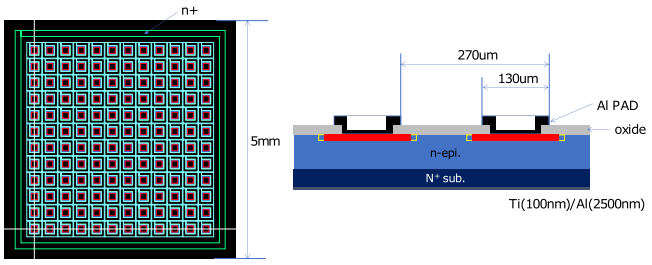

Fig. 1. Schematic and cross section of the p-n diode. The pixelized electrodes are merged in this work. The p+ anode and JTE region are indicated in red and yellow, respectively.

future radiation detectors with a comparable size of silicon, we first investigated the influence of the bulk defects on the radiation sensor characteristics, by minimizing the surface contribution to the leakage current with a relatively small-scale p-n junction structure. The primary concern is not in a single best device, but rather in a performance variation on the reverse blocking characteristics, leakage current, MIPs detection capability, and so on. By demonstrating the performance of those small protosensors, we aim to obtain the basic sensor properties that are critical for dedicated front-end electronics designs and also to establish the fabrication process for subsequent larger sensors. In this article, in Section II, we describe the fabrication process. In Section III, we report the I–V characteristics. In Section IV, we present the spectral studies using radioactive sources. In Section V, we discuss the possibility of the fabricated devices to the μ-beam monitor application. Finally, in Section VI, we present our conclusions.

II. Device Fabrication

First, p-n junction diodes with a reverse bias tolerance of over 3 kV were designed with a device simulator. Based on the simulation results, the device was fabricated in the prototyping facilities for power devices at the National Institute of Advanced Industrial Science and Technology (AIST) in Japan. The epitaxial layer was grown on a (0001) 4H-SiC n-type substrate. The effective doping density ($=N_d-N_a$) of the low doping n-type drift layer was estimated to be 4.7×10^{14} cm^{-3} from the C–V measurement using Hg, which was proved using a monitor wafer grown in the same batch. The thickness of the epitaxial layer was 52 μm and a reverse voltage of $\sim$1.2 kV was calculated for full depletion of the epitaxial layer.

The schematic and cross section of the p-n diode are shown in Fig. 1. The die size is 5 mm $\times$ 5 mm with an n+ field stop ring and a junction termination extension (JTE) structure for high reverse blocking capability in each pixel. The p-n diode consists of small cell-type p-n structures, which can be developed as needed for future hybrid pixel detectors. In this work, all pixelated diodes are merged into a single diode by connecting the electrodes with a common metal pad in order to increase the active area for MIPs detection. The sizes of Al metal pad and active diode areas are 3.1 mm $\times$ 3.1 mm and $\sim$0.1 cm^2, respectively. Low-pressure chemical vapor deposition (LPCVD) was used to generate a field oxide of 2-μm thickness to maintain a low reverse leakage current. The Al pad diameter was 130 μm, the width of the

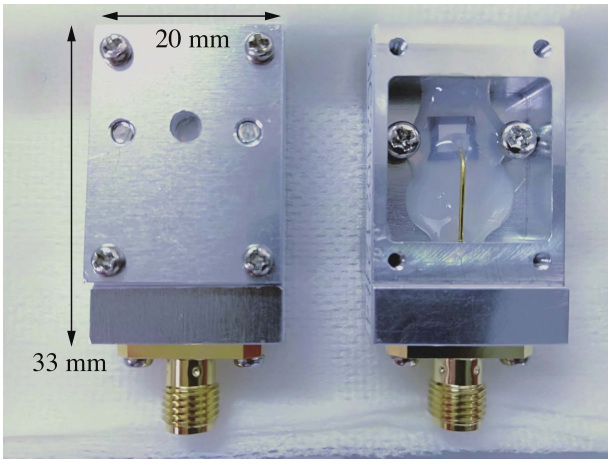

Fig. 2. Photograph of the fabricated device, mounted on an Al shielding box.

JTE structure was 40–50 μm, and the interval between each pixel was 20 μm. The typical diameter of each p-n structure was 160 μm. The p-well and p+ anode, including the JTE region, were formed by Al ion implantation at 500 °C. The activation annealing was carried out at 1800 °C for $\sim$5 min. Ohmic contact for top and backside electrodes was formed by an e-beam of Ni evaporation followed by postdeposition annealing at 900 °C for $\sim$1 min using an infrared rapid thermal annealing system. Al pads with 2.5-μm thickness were formed by metal sputtering.

III. I–V Characteristics

A. Device Implementation

The fabricated 4-in wafer was singulated into 260 dies. Among them, 10% of total dies, which was 26 samples, were randomly selected and implemented on an Al shielding box. Fig. 2 shows a photograph of the devices we investigated. The n-side was placed on the Al case and the p-side was connected to an SMA connector via an Au wire. In consideration of the scattering and absorption effects in spectroscopic studies with radioactive sources, a small hole of $\phi = 2$ mm was made on the shielding box and only the fringe of the n-side of the sensor was glued with an Ag paste for electrical contact. An Al cover with the same hole was attached with four M2 screws. Finally, the device was coated with silicone rubber (KER-2201; Shin-Etsu) as surface passivation to avoid electric discharges.

B. Leakage Currents

The I–V characteristics were measured at room temperature using a bias supply and a picoammeter (2410 & 6487; Keithley). Negative voltages of up to 1.1 kV were applied to the p-side of the diode, while the n-side was connected to the ground. The typical I–V characteristics are shown in Fig. 3. The leakage current shows a device-to-device dependence and is distributed between 1 and 8 nA at a reverse bias of 1 kV (corresponding to the leakage current density of 10–83 nA/cm^2). The fundamental reason for the distribution is beyond comprehension, and however,

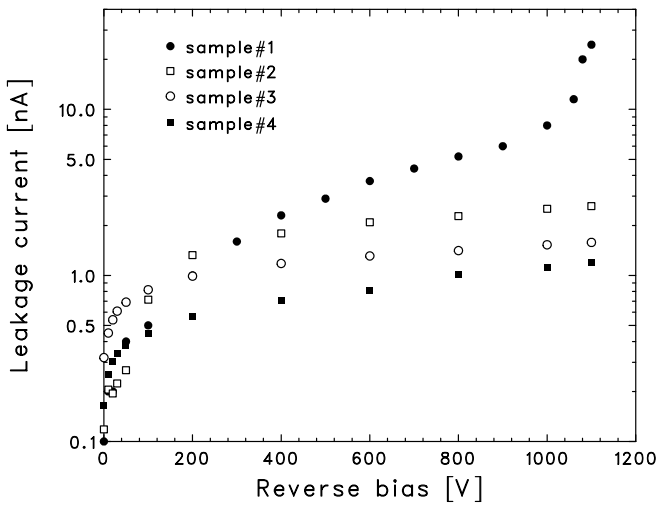

Fig. 3. Typical I–V characteristic of the randomly selected samples, measured at room temperature.

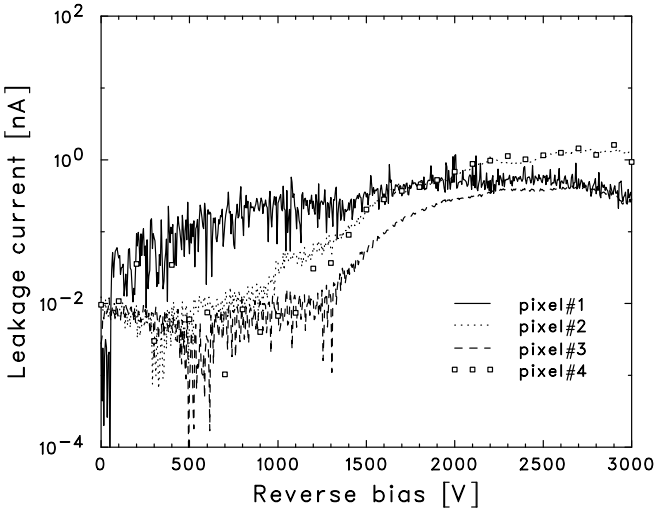

Fig. 4. Typical reverse blocking characteristics of the fabricated pixel diodes.

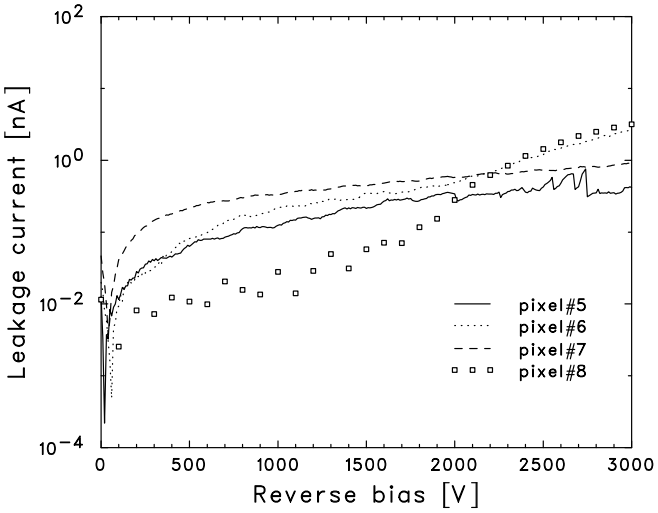

Fig. 5. Typical reverse blocking characteristics after 1-MeV neutron irradiation of 1.63×10^{13} n_{eq}/cm^2 fluence.

the bulk defects in the crystal are the natural interpretation. Compared with commercial SiC devices that are known as an integrated p-n Schottky structure [junction barrier Schottky (JBS)], the obtained leakage current and its distribution are suppressed in a wafer scale [18]. However, the objective of this work is not to compare with the leakage current of the Schottky diodes, but rather to study the variation of those values on signal detection capability or production yield for realistic MIP detectors. Among the Schottky diodes, there is an extremely low-current Schottky device fabricated by the intentionally nondoped epitaxial film and proper selection of barrier height [19]. We note that the device structure, such as the JTE structure, has much room for further reduction of the leakage current since the leakage current from the surface contribution is not completely excluded even in the p-n structure. Here, the relatively large and small leakage samples are labeled as samples #1 and #4 and referenced in Section IV. The breakdown starts above 1 kV in sample #1, while the flatness of the other samples remains constant up to 1.1 kV.

C. Reverse Blocking Characteristics on the Pixel Scale

In order to confirm the bulk defects on the intrinsic breakdown voltage, the monitor wafer (pixelized diodes) grown at the same batch was probed under dark conditions. Fig. 4 shows the typical reverse blocking characteristics in a 270 μm $\times$ 270 μm area encompassing several pixel diodes. Except for the pixel-to-pixel dependence, the avalanche blocking voltages over 3 kV were clearly confirmed on the pixel scale.

The reverse blocking characteristics is a primary concern of the radiation effects. The radiation-induced effects are generally divided into bulk and surface defects. The former are caused by the displacement of crystal atoms, introducing to the increase of the leakage current and degraded reverse blocking characteristics. The latter include all effects in the covering dielectrics and the interface region. Since the bulk damage caused by the elastic nuclear scattering of the lattice nuclei has a profound effect in our device, we irradiated 1-MeV neutrons to other pixelized devices under unbiased conditions. The irradiation test was conducted at the Institute for Integrated Radiation and Nuclear Science, Kyoto University. Details about the nuclear reactor and the irradiation setup can be found in [20]. Fig. 5 shows the typical leakage currents. Compared with Fig. 4, the bulk leakage current in reverse bias is not increased after neutron irradiation of 1.63×10^{13} n/cm^2 fluence, except for the pixel-to-pixel dependence and data fluctuation due to the different sampling time settings. The reverse blocking property was also retained up to 3 kV. Irradiation tests at higher fluences are severe with the current device structure due to the radioactivation of the metals. We note that the 1-MeV neutrons have the same efficiency in the detector degradation as 24-GeV protons at a comparable neutron equivalent fluence [2], [11]. The theoretical nonionizing energy loss (NIEL) calculation performed on SiC can be found in [21]. The primary radiation defects produced by single particles (protons and pions) or γ-rays were not evaluated in this measurement, and however,

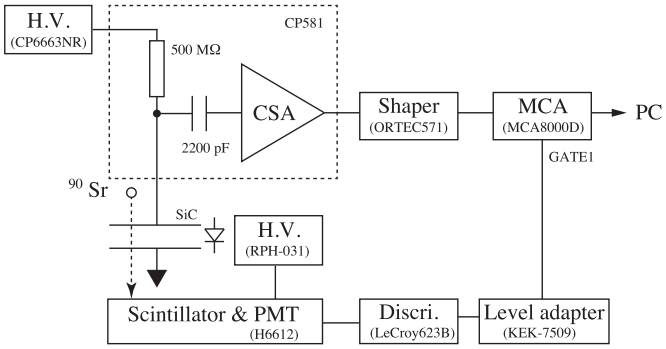

Fig. 6. Experimental setup for spectral studies.

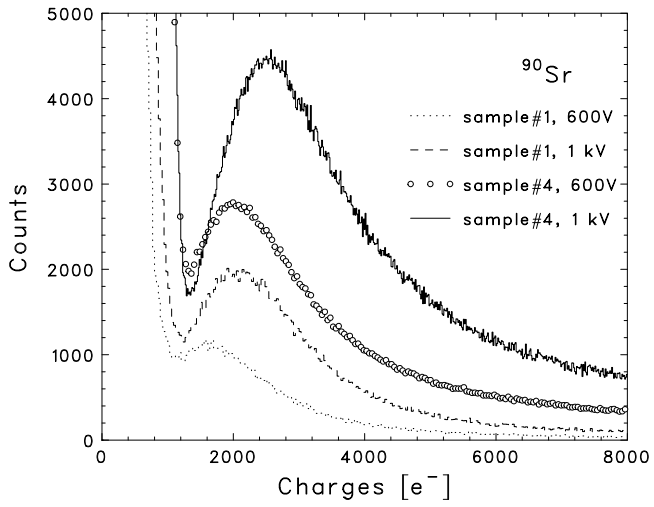

Fig. 7. ^{90}Sr β-ray spectra acquired at room temperature under different bias conditions.

the number of primary defects is reported as low as that of diamond [22]. Thus, we conclude that the bulk defects introduced by irradiation at the 10^{13} neutron equivalent fluence is ignorable, in agreement with the previous studies on neutron-irradiated p-n devices [9], [11], [23].

IV. Spectral Characteristics

A. Experimental Setup

The capability of MIP detection was investigated by using a commercial charge-sensitive amplifier (CSA) and a ^{90}Sr source; ^{90}Sr disintegrates through the emission of a β-ray with the maximum energy of 0.6 MeV to form ^{90}Y, while the daughter nucleus ^{90}Y is also a β-emitter of a continuous spectrum with an endpoint energy of 2.3 MeV. While most of the lower energy electrons are blocked by the surface passivation or electrodes, only the minimum ionizing electrons ($E_e > 1.5$ MeV) induce the signals in the sensor. A relativistic single charged particle generally penetrates deeply into the device, producing roughly uniform electron–hole pair densities along its path so long as the velocity remains relativistic. This energy loss in a sample can be treated in the Landau distribution and depends on the square of the particle charge but very weakly on the particle mass. Therefore, the induced signals from the ^{90}Sr β-ray source mimic the MIP events in SiC. Here, samples #1 and #4 in Fig. 3 were used, as reference samples of relatively large and small leakage currents. Fig. 6 shows the setup of the spectral measurements. The sensor signals were processed with a CSA (CP581; CLEARPULSE) and a shaping amplifier (571; ORTEC). The voltage outputs from the shaper were recorded with a multichannel analyzer (MCA8000D; Amptek). We note that the connection between the device and the CSA was in an ac-coupled scheme to protect the CSA from electrical discharges. To efficiently detect energetic electrons that pass through the SiC, a plastic scintillator was placed under the SiC sensor. The scintillator was read out by a PMT (H6612; HPK). The scintillator's hit signals were inserted to the MCA as a gate signal. The charge calibration from the MCA channels to the amount of charge in the SiC devices was performed using the pedestal peak and calibration test pulses into an internal capacitor of 1 pF equipped inside the CSA. The test pulse injection was performed with square waveforms having different voltage amplitudes using a voltage attenuator (2701; Tektronix) and a function generator (81130A; Agilent).

The charge calibration from the MCA channels to the amount of charges in the SiC devices was performed by using the pedestal and calibration test pulses. An internal capacitor of 1 pF of the CSA was utilized for the test pulse injection. By using a voltage attenuator (2701; Tektronix) and a function generator (81130A; Agilent), square waveforms with different voltage amplitudes were injected into the CSA. The voltage outputs of the amplified signals were recorded by the MCA. Although the absolute values of injected charges are uncertain, a linear curve can be uniquely determined from the test pulse data and the pedestal peak as the point of origin. This is based on an assumption that the ratios among pseudo-charges by test pulses are relatively accurate, while a certain amount of uncertainty exists in the absolute charges of injected test pulses.

B. MIPs Detection With ^{90}Sr Spectra

Fig. 7 shows the spectra of samples #1 and #4, which were obtained with a ^{90}Sr β-ray source under different bias conditions. All measurements were performed at room temperature. The horizontal units were converted from MCA channels to charge amounts using the calibration curves. The shaping time was fixed at 3 μs during the spectral measurements, under the condition of the smallest full-width at half-maximum (FWHM) in the test pulse distribution. Since the Landau peaks are clearly observed even with a relatively large leakage current device, the variation of the leakage currents does not have a significant influence on the MIPs detection. The samples showed repeatable spectra and the polarization effect was not observed during the measurement over several consecutive weeks.

The Landau peak position shifts to the right with larger bias voltages. This trend corresponds to larger signal charges due to the thicker depletion width. The applied bias dependence of the Landau peak is shown in Fig. 8. The peak position was determined by fitting the spectra with a Landau function in the

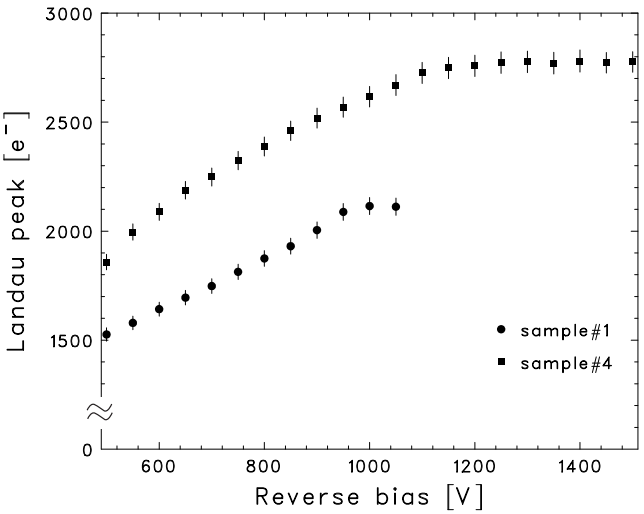

Fig. 8. Landau peaks as a function of the applied reverse bias voltage.

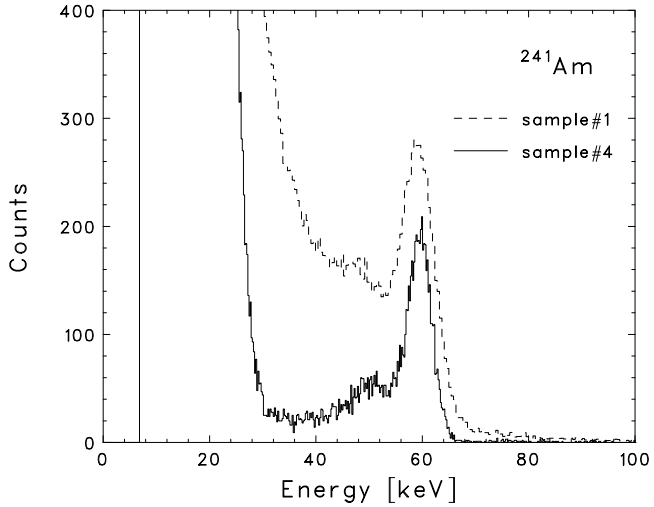

Fig. 9. ^{241}Am γ-ray spectra acquired at room temperature with a reverse bias voltage of 600 V.

range of 1400–5000 e^-, and most probable (mean) values are plotted in the figure. From the position saturation region, full depletion is speculated to occur around 1.2 kV in sample #4, while the same occurs at 1 kV in sample #1. The difference of the Landau peaks at the full depletion indicates the device dependence of the depletion layer widths. The difference of ~20% can be explained by the dispersion in the doping profile. The measurement of sample #1 was limited to 1.1 kV due to the large leakage current around the diode breakdown. Thus, the acceptable range of the leakage current for the MIP detection is deduced as approximately 10 nA/0.1 cm^2.

The Landau peaks of samples #1 and #4 correspond to 2038–2190 e^- at 1 kV and 2718–2912 e^- at 1.3 kV, respectively. Considering a value of 55 e^- for the number of electron–hole pairs per μm for MIPs in p-n-type SiC devices [9] and assuming that the effective doping density of an epitaxial layer is constant in depth and in-plane distribution, the depletion layer width is estimated to be 37–40 μm and 49–53 μm for samples #1 and #4, respectively. Thus, the measured bias voltage of sample #4 in full depletion was in good agreement with the initially designed value of 52 μm. Thus, we concluded that almost 100% CCE is achieved in sample #4. The diode capacitance at the full depletion was checked as 29.4 $\pm$ 0.1 pF with a commercial C–V meter (7500; CLEAR-PULSE).

C. Pair Creation Energy With ^{241}Am Spectrum

The electron–hole pair creation energy ϵ was determined by combining the calibration curves with the ^{241}Am γ-ray source. The gate signals from a scintillator to the MCA were disabled in this measurement. Fig. 9 shows the spectra of ^{241}Am. The measurements were performed at room temperature with a reverse bias voltage of 600 V. Monoenergetic 59.5 keV peaks of ^{241}Am were clearly observed with the FWHM of 8.63 and 5.43 keV for samples #1 and #4, respectively. Although the obtained values are much worse than those in the previous studies [15], [24], we note that the energy resolution or total noise performance is mainly dominated by the performance of readout electronics, which depends on the sensor capacitance, shaping time, and/or implementation between the sensor and electronics connection, i.e., ac or dc connection. Since the spectral widths were consistent with the pedestal distribution including the diode, the signal deterioration due to charge traps in the bulk defects can be ignored in the charge collection. Thus, the difference of the FWHMs is interpreted as a characteristic of leakage current. The value of ϵ was estimated by the calibration curve to be 7.36–7.83 eV, which is consistent with the previous report [15].

V. Future Prospects: Application to the COherent Muon-to-Electron Transition (COMET) Muon Beam Monitor

Our devices have demonstrated the MIPs detection and spectroscopic capabilities irrespective of the leakage currents with stable operation. This result overcomes the low production yield or small active area of SiC devices and provides a multisensor approach to cover the comparable area of a single silicon sensor. Charged particle beam monitors in HEP experiments are valid for such applications since the replacement of running silicon or the new detector installation with higher radiation tolerance and comparable active area is a primary concern in most facilities. Since the initial p-n fabrication process has been proven, here, we discuss the feasibility of application to the μ-beam monitor in the COMET experiment at Japan Proton Accelerator Research Complex (J-PARC) [25]. We stress that the obtained basic device properties are also quite useful for designing dedicated front-end electronics and for the feedback to the process parameters and/or sensor structures of subsequently larger devices.

The experiment aims to search for neutrinoless muon-to-electron conversion processes in the field of the nucleus, e.g., $\mu^- + (A, Z) \rightarrow e^- + (A, Z)$, as a charged lepton flavor violation process. Fig. 10 shows the overview of the detectors and beamlines during the physics measurement in the COMET Phase-I experiment. The μ-beams are generated from the decay of pions, which are generated by the primary proton

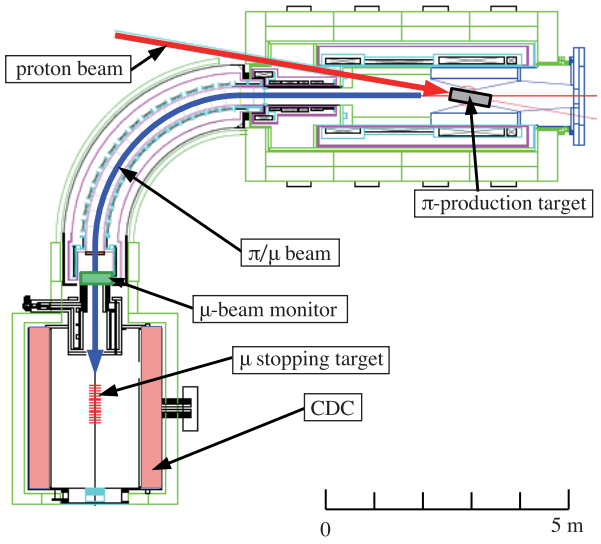

Fig. 10. Layout of detectors and beamlines during the physics measurement in the COMET Phase-I experiment.

beam collisions with the pion-production target. The pions are then collected by the solenoidal field and transported to the main detectors during the decay to muons. Monoenergetic electrons from muon decay are emitted from the μ-stopping target and detected by a cylindrical drift chamber (CDC).

The planned μ-beam monitor will be inserted in a vacuum chamber and located in front of the μ-stopping target and the CDC. The μ-beam monitor plays a key role in tracking the beam intensity and spatial stability of the secondary μ-beams and is also used for the particle identification of the background. The main requirements of the monitor are as follows: 1) relatively large area of $\approx$250 cm^2 to cover the 1σ beam spot and 2) a radiation tolerance with $\approx 5 \times 10^{13}$ neutron equivalent fluence. In this application, the signal charges are sufficiently larger than a single MIP because of the multiple particles of the high-intensity beams. In terms of detector size and space in the vacuum chamber, semiconductor sensors or scintillation fibers are popular choices among various MIP detectors. Since detector replacement during the operation is constrained due to the location within the vacuum chamber, the latter option is excluded due to radiation intolerance. Among the semiconductor detectors, an n-type silicon is a standard option in HEP experiments, and however, there are risks of signal deterioration with increasing leakage current during the irradiation. The substrate-type inversion also requires consideration in silicon after irradiation of $\approx 10^{13}$ neutron equivalent fluence, indicating that the widegap semiconductors are the realistic solutions. The diamond or GaN is, however, still required technological breakthroughs in production costs, sizes, and yields. SiC is thus thought to be a good candidate to meet the simultaneous demands of the active area and radiation tolerance.

To fulfill the active area, the SiC strip sensors are a good candidate. Contrary to silicon, however, it is not easy to obtain large and perfect SiC crystals. We thus plan to fabricate various strip sensors and study the leakage current and signal charges on larger scales in the next prototyping. We note that the area requirement can be fulfilled even with the current 5 mm $\times$ 5 mm dies by arraying in a 32$\times$32 matrix, singulated from four 4-in wafers. The influence of radiation on the charge trapping due to the induced bulk defects is not clear yet, and however, only a slight decrease on the charge collection is inferred from the irradiation on p-n-diode at a comparable neutron equivalent fluence in the previous studies [9], [11], [23]. Even in the case of unexpected I–V degradation during the experiment, there is still an option of device screening with sufficiently low leakage current characteristics under the preir-radiation condition. Rather, the radiation effect on the intense electric fields in the device should be carefully investigated by exposing them to the neutrons or charged particles under a consecutive bias condition of $\approx$1.2 kV. The next neutron irradiation tests will be conducted with fluence of up to 10^{16} 1-MeV neutrons (n)/cm^2 with the next prototype sensors with nonradioactivation metals.

VI. Conclusion

We fabricated SiC p+n junction diodes for MIP detectors at AIST in Japan. The devices were formed on an n-type substrate of a 4-in 4H-SiC wafer, and the epitaxial layer was grown with a low doping concentration of $N_{\rm d}-N_{\rm a} = 5 \times 10^{14}$ cm^{-3} to attain a sufficiently thick depletion layer. The fabricated devices have demonstrated MIP detection and spectroscopic capabilities irrespective of the leakage currents while maintaining stable operation. The bias dependence of the ^{90} Sr Landau peak indicates that the depletion layer width reaches the designed value of 52 μm at a reverse bias of 1.2 kV. The estimated electron–hole pair creation energy of 7.36–7.83 eV was also consistent with widely reported SiC devices, which we expect a superior radiation tolerance in harsh radiation environments. We conclude that the investigated p-n diodes have sufficient MIPs detection capability and are applicable to the beam monitor applications in the COMET experiment at J-PARC.

Acknowledgment

The authors would like to thank Masayuki Hagiwara and Hiroshi Yashima for coordinating the neutron irradiation test and the use of the facility.

References

[1] T. Seyller, "Electronic properties of SiC surfaces and interfaces: Some fundamental and technological aspects," *Appl. Phys. A, Solids Surf.*, vol. 85, no. 4, pp. 371–385, Oct. 2006.
[2] F. Nava, G. Bertuccio, A. Cavallini, and E. Vittone, "Silicon carbide and its use as a radiation detector material," *Meas. Sci. Technol.*, vol. 19, no. 10, Oct. 2008, Art. no. 102001.
[3] R. V. Babcock, S. Ruby, F. Schupp, and K. Sun, "Miniature neutron detectors," Westinghouse Elec. Corp., Pittsburgh, PA, USA, Tech. Rep. 5711-6600-A, 1957.
[4] R. V. Babcock and H. C. Chang, "SiC neutron detectors for high temperature operation," in *Proc. IARA Symp.*, vol. 1, 1963, p. 613.
[5] F. H. Ruddy, A. R. Dulloo, J. G. Seidel, S. Seshadri, and L. B. Rowland, "Development of a silicon carbide radiation detector," *IEEE Trans. Nucl. Sci.*, vol. 45, no. 3, pp. 536–541, Jun. 1998.
[6] M. Rogalla, K. Runge, and A. Soldner-Rembold, "Paticle detectors based on semi-insulating silicon carbide," *Nucl. Phys. B, Proc. Suppl.*, vol. 78, pp. 516–520, Aug. 1999.

[7] T. Dubbs *et al.*, "Development of radiation-hard materials for microstrip detectors," *IEEE Trans. Nucl. Sci.*, vol. 46, no. 4, pp. 839–843, Aug. 1999.
[8] S. Sciortino, S. Lagomarsino, and F. Nava, "Silicon carbide for high signal to noise ratio MIPs detection from room temperature to 80°C," *IEEE Trans. Nucl. Sci.*, vol. 56, no. 4, pp. 2538–2542, Aug. 2009.
[9] F. Moscatelli, A. Scorzoni, A. Poggi, and M. Bruzzi, "Radiation hardness after very high neutron irradiation of minimum ionizing particle detectors based on 4H-SJC p^+n junctions," *IEEE Trans. Nucl. Sci.*, vol. 53, no. 3, pp. 1557–1563, Jun. 2006.
[10] F. Nava, A. Castaldini, A. Cavallini, P. Errani, and V. Cindro, "Radiation detection properties of 4H-SiC Schottky diodes irradiated up to 10^{16} n/cm^2 by 1 MeV neutrons," *IEEE Trans. Nucl. Sci.*, vol. 53, no. 5, pp. 2977–2982, Oct. 2006.
[11] J. M. Rafi *et al.*, "Electron, neutron, and proton irradiation effects on SiC radiation detectors," *IEEE Trans. Nucl. Sci.*, vol. 67, no. 12, pp. 2481–2489, Dec. 2020.
[12] F. Nava *et al.*, "Minimum ionizing and alpha particles detectors based on epitaxial semiconductor silicon carbide," *IEEE Trans. Nucl. Sci.*, vol. 51, no. 1, pp. 238–244, Feb. 2004.
[13] G. Bertuccio, R. Casiraghi, A. Cetronio, and C. Lanzieri, "Low-noise silicon carbide X-ray sensor with wide operating temperature range," *Electron. Lett.*, vol. 40, no. 3, pp. 173–174, Feb. 2004.
[14] G. Bertuccio *et al.*, "Ultra low noise epitaxial 4H-SiC X-ray detectors," *Mater. Sci. Forum*, vols. 615–617, pp. 845–848, Mar. 2009.
[15] G. Bertuccio and R. Casiraghi, "Study of silicon carbide for X-ray detection and spectroscopy," *IEEE Trans. Nucl. Sci.*, vol. 50, no. 1, pp. 175–185, Feb. 2003.
[16] D. Puglisi and G. Bertuccio, "Silicon carbide microstrip radiation detectors," *Micromachines*, vol. 10, no. 12, p. 835, Nov. 2019.
[17] B. F. Phlips *et al.*, "Silicon carbide PiN diodes as radiation detectors," in *Proc. IEEE Nucl. Sci. Symp. Conf. Rec.*, Oct. 2005, pp. 1236–1239.
[18] P. A. Ivanov *et al.*, "Leakage currents in 4H-SiC JBS diodes," *Semiconductors*, vol. 46, no. 3, pp. 397–400, Mar. 2012.
[19] G. Bertuccio, S. Caccia, R. Casiraghi, and C. Lanzieri, "Possibility of subelectron noise with room-temperature silicon carbide pixel detectors," *IEEE Trans. Nucl. Sci.*, vol. 53, no. 4, pp. 2421–2427, Aug. 2006.
[20] Kyoto University Research Reactor. Accessed: Feb. 10, 2021. [Online]. Available: https://www.rri.kyoto-u.ac.jp/en/facilities/hl
[21] K. K. Lee, T. Ohshima, A. Saint, T. Kamiya, D. N. Jamieson, and H. Itoh, "A comparative study of the radiation hardness of silicon carbide using light ions," *Nucl. Instrum. Methods Phys. Res. Sect. B, Beam Interact. with Mater. At.*, vol. 210, pp. 489–494, Sep. 2003.
[22] A. A. Lebedev, A. M. Ivanov, and N. B. Strokan, "Radiation resistance of SiC and nuclear radiation detectors based on SiC films," *Semiconductor*, vol. 38, pp. 125–147, Feb. 2004.
[23] F. Nava, E. Vittone, P. Vanni, P. G. Fuochi, and C. Lanzieri, "Radiation tolerance of epitaxial silicon carbide detectors for electrons and γ-rays," *Nucl. Instrum. Methods Phys. Res. A, Accel. Spectrom. Detect. Assoc. Equip.*, vol. 514, nos. 1–3, pp. 126–134, Nov. 2003.
[24] K. C. Mandal, P. G. Muzykov, S. K. Chaudhuri, and J. R. Terry, "Low energy X-ray and γ-ray detectors fabricated on n-type 4H-SiC epitaxial layer," *IEEE Trans. Nucl. Sci.*, vol. 53, no. 4, pp. 2421–2427, Aug. 2006.
[25] R. Abramishvili, "COMET phase-1 technical design report," *Prog. Theor. Exp. Phys.*, vol. 2020, no. 3, Mar. 2015, Art. no. 033C01, doi: 1093/ptep/ptz125.